CONF-9404286--1
SAND95-2108C

PHOTO- AND CATHODOLUMINESCENCE OF HYDROTHERMALLY SYNTHESIZED $Y_3Al_5O_{12}$:Tb AND $NaY(WO_4)_2$:Tb

Mark L. F. Phillips and B. G. Potter, Jr.
Sandia National Laboratories, Albuquerque, NM 87185

ABSTRACT

Cathodoluminescent (CL) phosphors with improved low-voltage characteristics are needed for use in emissive flat panel displays. Conventional high-temperature methods for phosphor synthesis yield large polycrystalline grains that must be pulverized prior to screen deposition. Grinding has been implicated in reducing phosphor efficiency by causing surface contamination and defects. Hydrothermal synthesis has been used to improve the quality of ceramic powders by producing fine, well-formed crystallites without grinding. Two green-emitting phosphors, $Y_3Al_5O_{12}$:Tb (YAG:Tb) and $NaY(WO_4)_2$:Tb, were used to test the effects of hydrothermal synthesis on grain size and morphology, and on low-voltage CL properties. YAG:Tb prepared hydrothermally consisted of submicron crystallites with a typical garnet habit. The CL efficiency of hydrothermally synthesized YAG:Tb (3 lm/W at 800 V) was comparable to that of equivalent YAG:Tb compositions prepared via high-temperature solid state reaction. In comparison, CL intensities of $Gd_3Ga_5O_{12}$:Tb were slightly better (3.5 lm/W at 800 V), while those of $NaY(WO_4)_2$:Tb were approximately 1/100th that of YAG:Tb. Both CL and photoluminescence data show that the difference in the cathodoluminescence of YAG and $NaY(WO_4)_2$ can be understood in terms of differences in the mechanism of activation.

1. INTRODUCTION

Field emission-based displays (FEDs) are beginning to compete with liquid crystal displays (LCDs) for direct-view flat panel display applications. Full color FEDs are expected to offer several advantages over LCDs, including lower power consumption, lower manufacturing costs, and improved screen appearance through wider viewing angle and enhanced resolution and brightness. FEDs use electron beams to excite cathodoluminescent phosphors deposited on a screen, as conventional cathode ray tube (CRT) displays do. But while a CRT display rasters a beam from a single thermionic electron gun (or three guns, if in full color) across a phosphor screen, a FED uses an array of microscopic cold cathodes to irradiate the screen. Such arrays can contain as many as 10^7 emitters/cm^2, so that thousands

DISCLAIMER

Portions of this document may be illegible in electronic image products. Images are produced from the best available original document.

of emitters can be used to illuminate a single pixel.[1]

FEDs also differ from CRTs in that they operate at lower voltages. The electron guns in CRT displays produce electrons at high energy (typically 10-25 keV). Because the cold cathodes in an FED must be held a short distance from the screen to obtain adequate resolution, they must be operated at lower voltages in order to avoid vacuum breakdown. In order to maintain adequate screen brightness, the electron current must be increased to compensate for the decreased voltage. Phosphors for FEDs must therefore not only be efficient at low voltages, but also resistant to saturation and Coulomb aging at high current densities.

In order to compete with LCDs in terms of power consumption, full-color FEDs will need a three-color phosphor scheme with a white brightness efficiency of 2-3 lm/W. With good color saturation, this requires green, red, and blue phosphors with efficiencies of approximately 6, 3, and 1 lm/W, respectively. These efficiencies can be achieved at 500 V using sulfide phosphors such as Y_2O_2S:Eu (red, 3.5 lm/W), Zn,CdS:Cu,Al (green, 4.8 lm/W), and ZnS:Ag (0.8 lm/W).[2] However, sulfide phosphors can release sulfur-containing gases under low-energy electron irradiance.[3] In addition to damaging the phosphor grain, this degradation can contaminate the field emitter tips, changing their work functions and decreasing (or catastrophically increasing) emission current.[4]

Oxide phosphors are less likely to contaminate the atmosphere within the FED, but few oxide CL phosphors are as efficient as the sulfides. Most oxide phosphors tend to be inefficient at low voltages (less than ca. 500 V), and most exhibit a threshold voltage below which no light is emitted. This can be as high as 200-300 V.[5] Using higher current densities to compensate for loss of efficiency at low excitation voltage can also lead to saturation and/or damage. Dead voltage is caused principally by surface bound electrons (SBEs) and surface recombination (SR) centers. SBEs result from secondary electron emission and cause the surface of the phosphor grain to become negatively charged; this surface charge repels or deflects the incident electron beam. SR centers are surface defects at which excitons created by electron impact can recombine nonradiatively. These defects can be caused by surface contamination or defects introduced by grinding.[6]

ZnO:Zn is unusual among oxide phosphors in that it is both highly efficient (13 lm/W) and electrically conductive, and is luminescent with electron energies as low as 5 eV.[7] However, ZnO:Zn is susceptible to saturation (efficiency loss) at moderate current densities, and the blue-green visible emission from this phosphor has poor chromaticity values. Rare-earth doped phosphors have the advantage of using higher activator concentrations, which allow them to be used at higher electron currents before saturating. Saturation resistance is a requirement in projection CRTs, which frequently use $Y_3Al_5O_{12}$:Tb (YAG:Tb) as a green-emitting phosphor.[8] The low-voltage cathodoluminescence of YAG:Tb and its isostructure $Gd_3Ga_5O_{12}$:Tb (GGG:Tb) are studied in this work. Another rare-earth host, $NaY(WO_4)_2$, was also studied as a CL phosphor. This phase is isostrucural with

the fluorescent mineral scheelite, $CaWO_4$, and has been studied as an anti-Stokes phosphor when codoped with Yb and Er, Tb, or Tm, and as a laser host when doped with Nd.[9] The high photoluminescent (PL) efficiency of $NaY(WO_4)_2$:Tb and the similarity of its emission spectrum to that YAG:Tb warrant an investigation of its low-voltage CL properties.

Hydrothermal synthesis is a route to producing well-crystallized oxide powders with good control over particle size distribution. This process can yield fine particles without grinding, and thus may reduce surface defects, contamination, and threshold voltage. In addition, the very fine (1 μm or smaller) particle sizes available allow smaller pixel sizes, which are needed in high resolution displays such as projection CRTs. Phosphors and host phases that have been synthesized hydrothermally include YAG:Tb,[10,11] $ZnGa_2O_4$,[12] Zn_2SiO_4:Mn,[13] Y_2O_3,[14] and YVO_4:Eu.[15]

In this work both photoluminescence and low-voltage cathodoluminescence are studied in YAG:Tb and $NaY(WO_4)_2$:Tb phosphors. These materials were synthesized via both hydrothermal and conventional high-temperature solid state routes to determine whether hydrothermal synthesis affects CL efficiency, particularly at low voltages, and if this method can be used to obtain phosphor powders with finer grain sizes. The hydrothermal synthesis of $NaY(WO_4)_2$ and the CL properties of hydrothermally synthesized YAG:Tb are reported here for the first time. The mechanisms of activation in YAG:Tb and $NaY(WO_4)_2$:Tb and their effects on CL efficiency are also investigated and compared.

2. EXPERIMENTAL

2.1 Synthesis

$Y_3Al_5O_{12}$:Tb and $Gd_3Ga_5O_{12}$:Tb powders were prepared by high temperature solid state reaction:[16] Y, Tb, and Al oxide precursors were combined in stoichiometric proportion, pre-reacted at 1200 °C for 18 hr, reground, and annealed at 1450 °C for 6 hr. The YAG:Tb compositions were also synthesized hydrothermally using a method similar to that described in ref 10, starting with nitrate salts of Y, Al, and Tb. The Tb/Y ratio in the starting material was equal to that in the desired product, while Y and Tb were added in excess of the (Y:Tb)/Al product stoichometry. The excess rare earth was necessary to prevent formation of α–Al_2O_3, since YAG saturates incongruently in water.[11] The Y, Al, and Tb salts were dissolved in water, then hydrolyzed by adding aqueous NH_3 until a pH of 10 was reached. The resulting gels were then filtered, dried at 150 °C, and heated at 500 °C for 6 hr in N_2. This yielded amorphous YAG:Tb precursors that were then ground, individually sealed in Au tubes with an equivalent weight of water, and autoclaved at 600 °C and 3.20 kbar for 24-32 hr. Products were recovered by filtration, using Gelman 0.22 μm membrane filters. Portions of the hydrothermally synthesized YAG:Tb samples were annealed at 1200 °C and 1450 °C.

$NaY(WO_4)_2$:Tb compositions were synthesized at high temperature by combining

stoichiometric quantities of Y_2O_3, $Tb(NO_3)_3 \cdot 5H_2O$, Na_2WO_4, and WO_3, then heating the mixture to 1000 °C. These phases were also prepared hydrothermally by reacting solutions of Y and Tb nitrates with Na_2WO_4 in water at 200 °C and 15 bar. Portions of the hydrothermally synthesized samples were annealed at 900 °C.

2.2. Characterization

Particle sizes were determined by scanning electron microscopy (SEM) and by sedimentation. Samples for SEM were sputtered with Au and analyzed using an AMRAY model 1645 electron microscope. Particle size determination by sedimentation was accomplished by suspending the powder samples in a sodium pyrophosphate solution, sonicating, and measuring settling rates using a Horiba CAPA-700 particle size analyzer. Powder X-ray diffraction (XRD) data were collected using a Scintag Pad V diffractometer. Crystallite sizes were calculated from the widths of the (420) and (101) diffraction peaks of $Y_3Al_5O_{12}$ and $NaY(WO_4)_2$, respectively, using a LaB_6 standard.

Photoluminescence (PL) and photoluminescence excitation (PLE) spectra were collected from the phosphor powders at room temperature using a computer-driven monochromator system. The output from a tunable excitation source (Xe arc lamp coupled to a 0.15 m monochromator equipped with order-sorting filters) was imaged to a spot size of approximately 0.8 x 5 mm at the sample with a spectral bandpass of 4 nm. PL spectra were acquired at an excitation wavelength of 254 nm. During PLE data collection, the 0.15 m (excitation source) monochromator slits were set to produce a 2 nm spectral bandpass. The resulting luminescence was analyzed using a 0.275 m single-pass monochromator equipped with a photomultiplier tube detector. The collection monochromator resolution was typically 0.5 nm for the survey spectra obtained. A lock-in amplifier and mechanical chopper provided phase-sensitive detection of the optical signal. Fluctuations in the lamp output were mediated using a beam splitter in the excitation beam path to divert a portion of the incident beam to a separate Si photodiode. The output of this detector was used to normalize the luminescence signal during data acquisition.

Cathodoluminescence data were collected in a vacuum chamber evacuated to 4×10^{-6} Pa. A hot filament, low-energy electron gun (Kimball Physics) was the source of the beam, which was steered and focused using external Helmholtz coils. The powder samples were packed approximately 1 mm deep into stainless steel cups. During analysis the sample cup was maintained at a potential of +30 V with respect to ground. The electron beam was focused onto a spot 4.5 mm in diameter. Light emitted from the sample was transmitted to a spectroradiometer (Oriel), which measured radiant energy as a function of wavelength.

3. RESULTS

3.1. Synthesis

In the course of hydrothermal processing the amorphous YAG precursor gel crystallizes to form regular grains with a garnet habit. Grains consist of

Figure 1a: Hydrothermally synthesized YAG:Tb powders (scale bar = 0.375 μm).

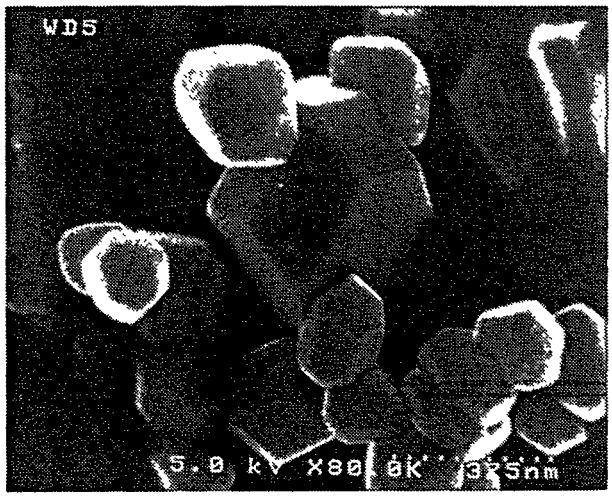

Figure 1b: Hydrothermally synthesized YAG:Tb, annealed at 1450 °C (scale bar = 1 μm).

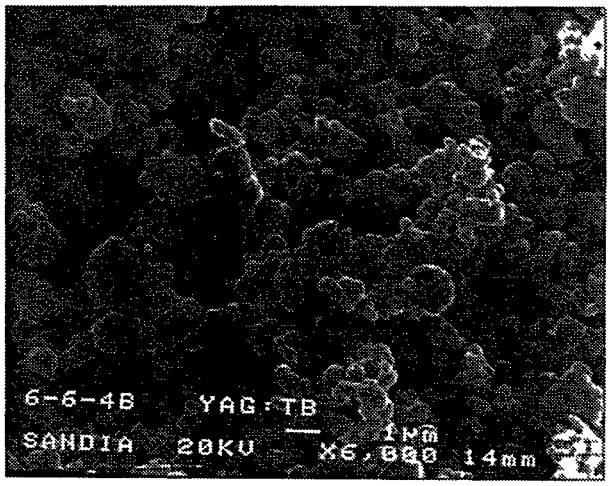

Figure 1c: Hydrothermally synthesized YAG:Tb grains from over-nucleated precursor gel (scale bar = 1 μm).

well-formed YAG:Tb crystallites with particle diameters between 0.2 and 2 μm, with the largest mass fraction at 0.5 μm (Figure 1a). These crystallites showed little tendency to agglomerate, and could be readily suspended in water through sonication. Minor sintering of smaller crystallites was evident at 1200 °C, while the powders annealed at 1450° were heavily sintered (Figure 1b).

It is pointed out in ref. 10 that if the YAG:Tb gel is heated beyond ca. 600 °C, it will become excessively nucleated, though the powder will remain X-ray amorphous until it is heated to ca. 900 °C. To determine the effect of crystallization of the precursor gel on the product YAG:Tb grains, a YAG:Tb precursor gel was heated to 700 °C, yielding a powder that is X-ray amorphous. This material was autoclaved in water in the same fashion as the amorphous gel. The resulting YAG:Tb powder consisted of rough polycrystalline grains with a crystallite size of 56 nm (Figure 1c). This result is likely due to increased nucleation density in the precursor, and possibly to decreased solubility of crystalline YAG in water versus the YAG precursor gel.

High-temperature synthesis of YAG:Tb via the solid state yields irregular grains with a typical diameter of 5 μm. These grains give the appearance of sintered microcrystallites in SEM views (Figure 2a). The effective crystallite size of YAG:Tb prepared at 1200 °C is 53 nm. Annealing at 1450 °C causes further sintering to yield crystallites with an average diameter of 320 nm (Figure 2b).

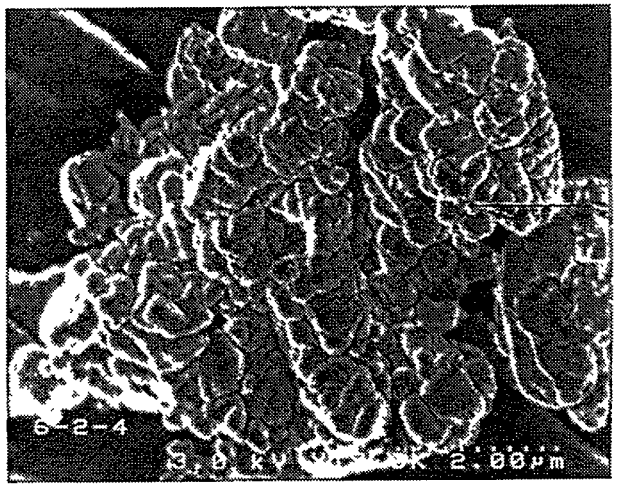

Figure 2a: YAG:Tb grain synthesized via solid state reaction at 1200 °C (scale bar = 2 μm).

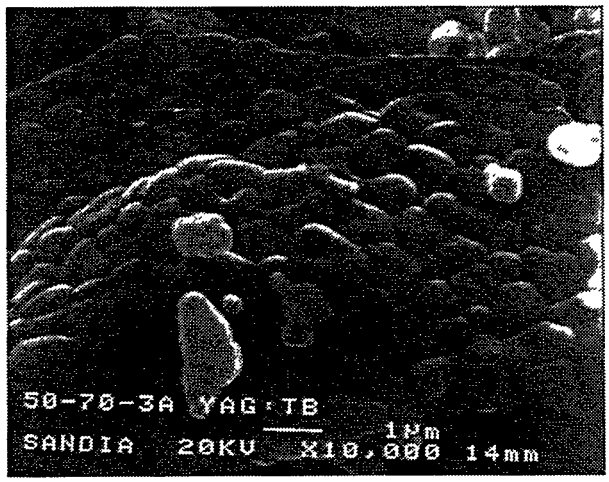

Figure 2b: Solid-state YAG:Tb, annealed at 1450 °C (scale bar = 1 μm).

Hydrothermal synthesis of $NaY(WO_4)_2$:Tb yields particles consisting of intergrown plates (Figure 3a). The effective crystallite size in these particles is approximately 800 nm. Annealing at 900 °C causes intraparticulate sintering to yield grains several microns across (Figure 3b). The grains thus obtained have essentially the same size and morphology as those prepared via high-temperature solid state reaction.

Figure 3a: $NaY(WO_4)_2$:Tb grains, synthesized hydrothermally at 200 °C (scale bar = 10 μm).

3.2. Luminescence

The luminescence center in a phosphor may undergo excitation and emission through several different mechanisms. These are generalized here as direct activation, in which incident energy is absorbed and reradiated by localized species (such as an activator ion, sensitizer, or charge-transfer band) and indirect activation, in which incident energy creates an excitation in the host lattice that is subsequently transferred to the luminescence center. A phosphor that is capable of indirect activation can also be directly activated if the excitation energy is detuned from the host lattice absorption and is made coincident with allowed transitions in the activator ion. Using optical excitation (PL), both direct or indirect mechanisms can be probed by varying the excitation energy. For example, Y_2O_3:Eu can be directly activated using 300 nm light through electronic transitions in the Eu^{3+} dopant. Conversely, the phosphor is indirectly activated at 200 nm through host lattice absorption.[17]

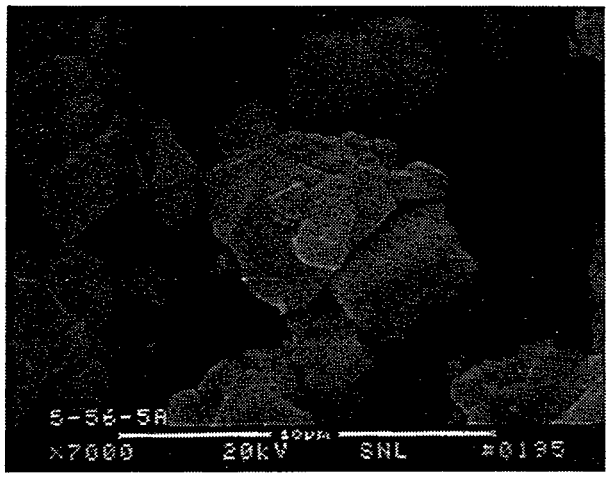

Figure 3b: Hydrothermally synthesized $NaY(WO_4)_2$:Tb after annealing at 900 °C (scale bar = 10 μm).

While both types of excitation may be accessed using PL, the cathodoluminescence process deposits energy only near the surface of a phosphor grain through inelastic scattering with lattice ions to produce secondary electrons, which then generate electron-hole pairs in the lattice. The excitation (in the form of electron-hole pairs) is then propagated through the host lattice to dopant ions within the grain interior to indirectly achieve activator excitation and radiative emission. Relative changes in the mean free path of this indirect excitation as it interacts with activator ions and microstructural features (such as defects, impurities, or grain boundaries) impact the luminescence efficiency of the phosphor. If recombination occurs nearly exclusively at an activator site, the average migration distance of the excitation will vary inversely with activator concentration. At lower activator concentrations (or smaller crystal sizes), migration distance and thus activation volume will be limited by crystal size, and at higher concentrations it will be limited by the density of activators. As activator concentration increases to the point where the density of activator ions begins to limit activation volume, PL and CL intensities becomes less sensitive to activator concentration.[18] This work examines the activation mechanisms for YAG:Tb and $NaY(WO_4)_2$:Tb phosphor powders with varied dopant concentrations through both PL and CL efficiency measurements.

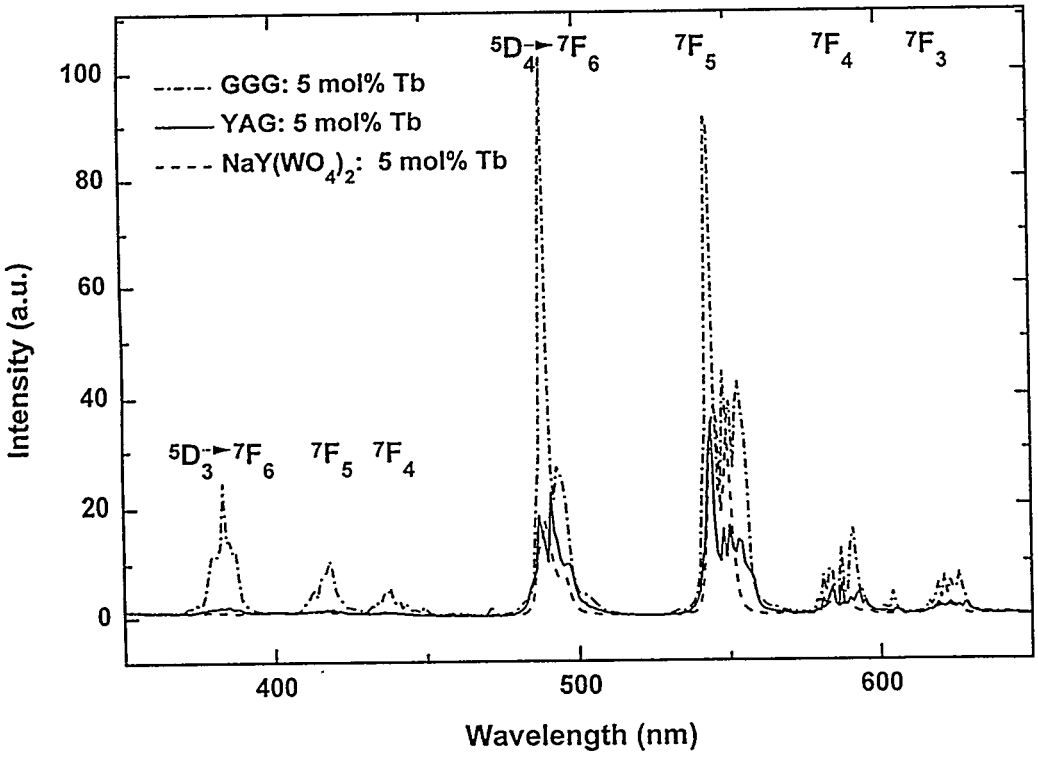

Figure 4: Photoluminescence spectra of $Y_3Al_5O_{12}$:Tb, $Gd_3Ga_5O_{12}$:Tb, and $NaY(WO_4)_2$:Tb, acquired using a 254 nm excitation source.

3.2.1. Photoluminescence: PL spectra (Figure 4) show that over the UV to visible wavelength range, the integrated luminescence intensities for $Y_{2.85}Tb_{0.15}Al_5O_{12}$, $Gd_{2.85}Tb_{0.15}Ga_5O_{12}$, and $NaY_{0.95}Tb_{0.05}(WO_4)_2$ increase in the order $NaY(WO_4)_2$ < YAG < GGG for excitation at 254 nm. Figure 5 shows the dependence of PL intensity on Tb concentration measured for the YAG and $NaY(WO_4)_2$ hosts. While the dependence of PL vs. concentration is steeper in $NaY(WO_4)_2$:Tb than in YAG:Tb, both hosts appear to reach similar intensity values at high dopant concentrations. A maximum integrated intensity was observed in the $NaY(WO_4)_2$ sample when 50% of the Y was replaced with Tb. This contrasts with the general increase in intensity observed in the YAG host over this concentration range. The $NaY(WO_4)_2$:Tb data appear linear (within error limits) until they exhibit a decrease for the sample with the highest Tb concentration. This is presumably due to concentration quenching effects. The linearity is indicative of the direct activation mechanism used in the experiment. No significant increase in integrated PL intensity was observed after the annealing treatments. This suggests that there was no significant change in activator local environment that led to a variation in transition oscillator strength.

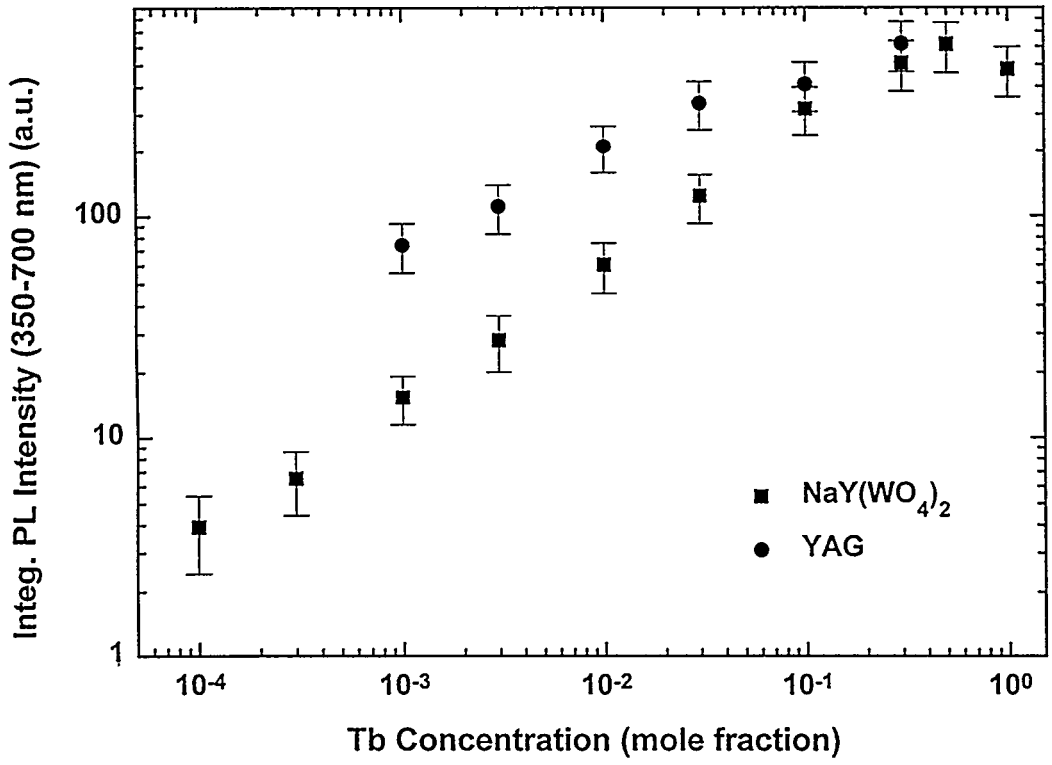

Figure 5: PL intensity vs. Tb concentration in $NaY(WO_4)_2$:Tb and $Y_3Al_5O_{12}$:Tb.

These initial conclusions regarding the excitation mechanisms in these phosphor samples were tested using photoluminescence excitation (PLE) measurements.

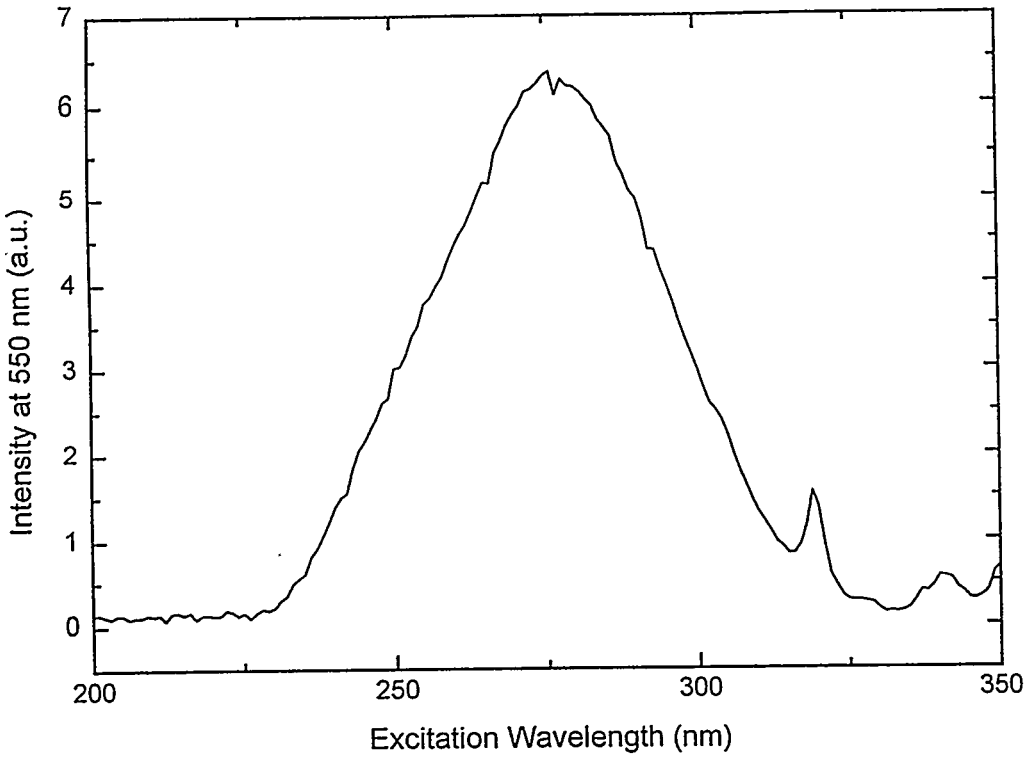

Figure 6: PL excitation spectrum of $NaY(WO_4)_2$:Tb, monitored at 550 nm.

Luminescence at 550 nm was monitored while scanning the excitation source. Figure 6 shows that a maximum in 550 nm output was observed with excitation near 275 nm for the $NaY(WO_4)_2$ host (similar results were obtained for the YAG host). This broad PLE band most likely results from a charge-transfer band absorption in the material. This is a localized excitation in the lattice, directly associated with the Tb dopant. Since luminescence occurs at the absorption site this a directly activated process. Smaller features at longer wavelengths correspond to direct, intra-ion excitation of the activator. Diffuse reflectance from the samples indicate absorption edge onset in the 220 to 250 nm range.[19] While no features are observed at shorter wavelengths in the PLE spectra, an estimation of the relative influence of host lattice absorption on the indirect excitation of Tb ions is not made here due to the significant decrease in excitation intensity available from the Xe lamp source at this wavelength range. Given the PLE data, however, it is apparent that the 254 nm excitation energy used in the PL experiment is directly activating the Tb dopant, which is in agreement with the concentration dependence of the integrated PL intensity.

3.2.2. Cathodoluminescence: CL efficiency data measured as a function of electron voltage at a constant power of 1.5×10^{-5} W for YAG:Tb and GGG:Tb powders are

presented in Figure 7. CL efficiency increases with voltage at constant power, approximately doubling between 150 and 1000 V. The threshold voltage for all phosphors was between 100 and 150V. The efficiencies of YAG:Tb prepared hydrothermally and via the solid state were similar to each other at all voltages, while those of GGG:Tb were greater by approximately 0.5 lm/W. The dead voltage and steep slope of the efficiency vs. voltage curve are most likely due to surface bound electrons: at higher voltages, luminance is higher at constant power due to increased penetration depth of the primary electron beam.

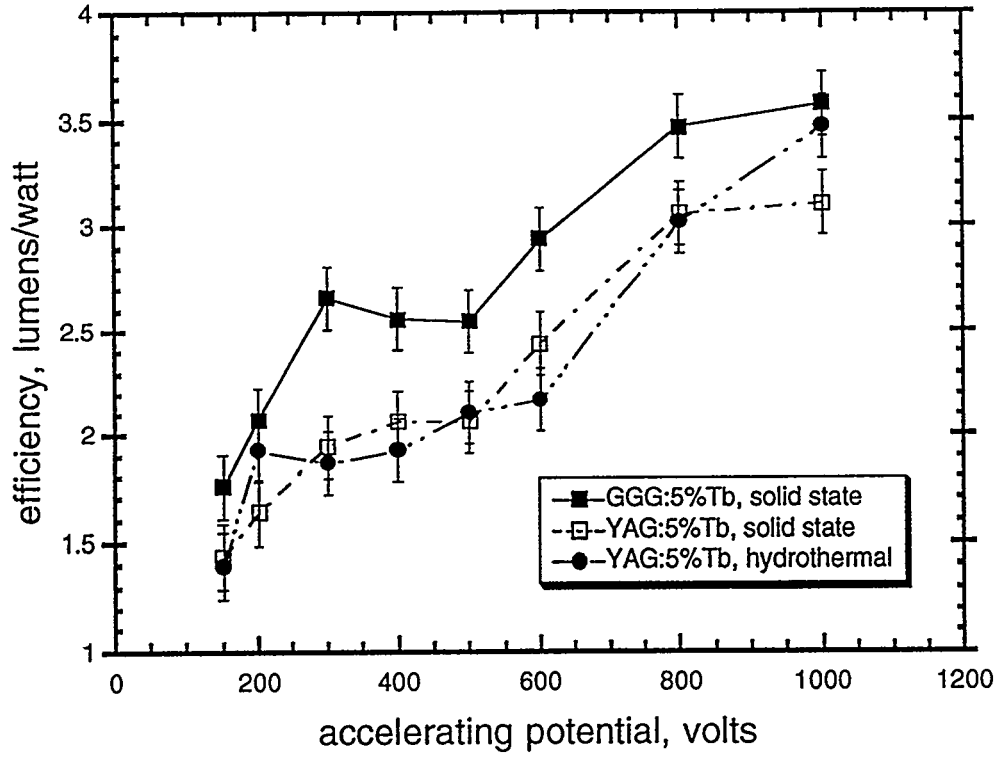

Figure 7: CL efficiencies of garnet phosphors as a function of electron energy.

Further insight into the excitation processes occurring in the YAG and $NaY(WO_4)_2$ samples was also obtained in the CL measurements. Figure 8 shows the relationship between CL efficiency and Tb concentration for YAG:Tb made via solid state reaction at 1200 °C, solid state YAG:Tb annealed at 1450 °C, and hydrothermal YAG:Tb annealed at 1200 °C. An accelerating potential of 800 V and beam power of 1.5×10^{-5} W was used for all data shown. The efficiencies of the annealed solid state and hydrothermal samples are similar at all concentrations, except that the samples made via the solid state are more susceptible to quenching at the highest dopant levels. Maximum efficiency is found at dopant concentrations between 5 and 10 mole percent in both solid state and hydrothermal YAG:Tb.

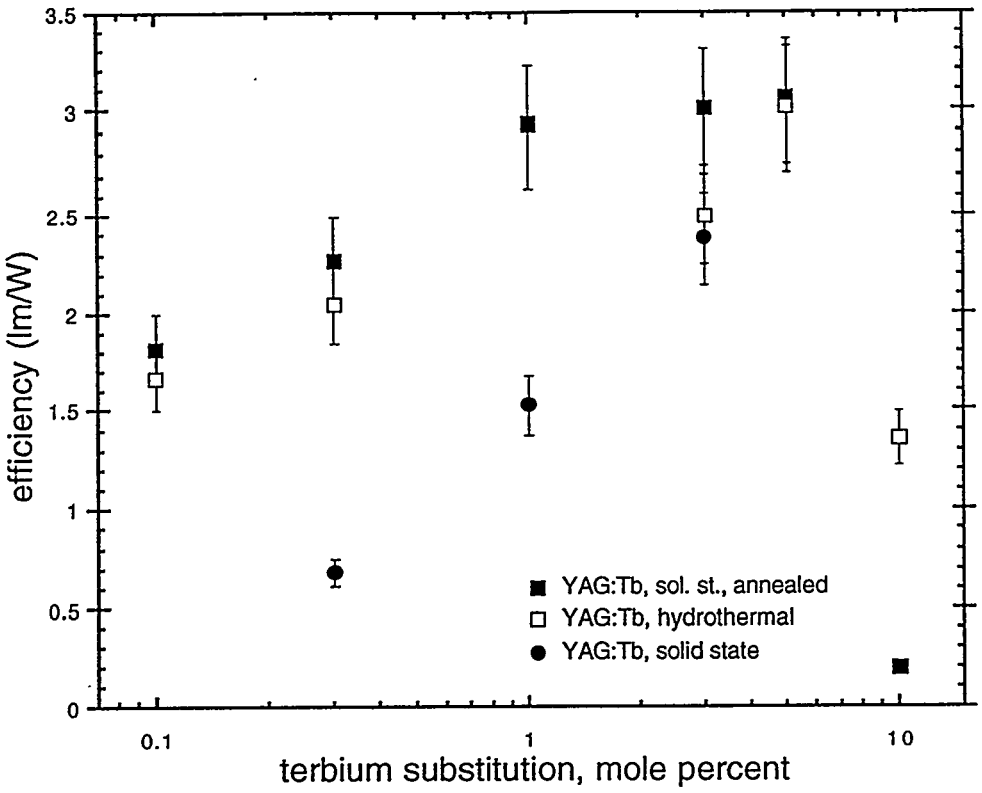

Figure 8: CL efficiency vs. activator concentration in $Y_3Al_5O_{12}$:Tb phosphors.

The slope of efficiency vs. Tb concentration for the unannealed solid state samples is approximately 2 lm/W per decade, while this dependence in the annealed samples is only ca. 1 lm/W per decade. This is probably due to the crystal size effect, which limits activation volume in the pre-annealed materials, causing increased sensitivity to activator concentration. The overall increase in CL intensity after annealing over the concentration range examined contrasts the PL data from the same samples in which no significant increase in intensity is observed. This indicates the increased influence of microstructure size on the excitation efficiency of the dopant in the CL measurement. This effect, coupled with the decreased dependence of CL intensity on concentration upon annealing, supports an indirect activation mechanism for the YAG:Tb.

The CL emission spectrum of $NaY(WO_4)_2$:Tb is essentially identical to that of YAG:Tb, but the luminescence of the former is much less efficient. The highest CL intensities observed for the $NaY(WO_4)_2$:Tb compositions were approximately 1% of that found for YAG:Tb. This again contrasts the PL studies, which show a much smaller difference in integrated luminescence intensity between the two host materials (particularly at the higher concentrations). The difference between the CL and PL trends reflects the predominant excitation mechanisms at work in these

studies. The significantly higher CL intensities for the YAG host indicate that it is indirectly activated by the electron beam much more efficiently than $NaY(WO_4)_2$, which appears to rely on direct activation of the Tb dopant in order to luminesce.

4. DISCUSSION

YAG:Tb and GGG:Tb are efficient CL phosphors at low voltages (< 1000 V). The PL and CL intensities from GGG:Tb were both greater than those from YAG:Tb; CL efficiencies as high as 3.5 lm/W were observed with GGG:Tb. By depositing these phosphors on conducting screens, it may be possible to further improve their performance, particularly at lower voltages (< 500 V). While the efficiency values reported here are still lower than those of the best green-emitting sulfide and oxysulfide phosphors, their excellent chromaticities and resistance to degradation and power saturation warrant consideration of garnet phosphors for use in field-emitter flat panel display screens.

Synthesizing YAG phosphors hydrothermally does not materially affect CL efficiency, so any reduction in surface recombination centers from low-temperature processing are probably not significant. It is more likely that surface-bound electrons are the principal cause of efficiency loss at lower voltages. Compared with conventional high-temperature processing, though, hydrothermal synthesis yields smaller crystallites of YAG with improved particle morphology. This would benefit projection CRT screens, which currently employ YAG:Tb as green-emitting phosphors.

The mechanism of cathodoluminescence requires transfer of absorbed electron energy from the host lattice to the activator, that is, a CL phosphor must be capable of being indirectly activated. While the PL intensities of Tb emission from YAG:Tb and $NaY(WO_4)_2$:Tb are similar, the CL efficiency of $NaY(WO_4)_2$:Tb is two orders of magnitude lower than that of YAG:Tb. These results strongly suggest that this phosphor can only be directly activated. While the low CL emission intensities from $NaY(WO_4)_2$:Tb may proscribe its use as a CL phosphor, its high PL efficiency may make it usable with UV-emitting phosphors as a wavelength shifter for lamps and displays.

5. ACKNOWLEDGMENTS

This work was supported by the U. S. Department of Energy under contract no. DE-AC04-94AL85000, and benefited from the assistance of R. J. Walko, R. Mays, G. R. Schuster, L. E. Shea, G. L. Zender, and D. L. Lamppa.

6. REFERENCES

1. *a.* I. Brodie and C. A. Spindt, "Vacuum Microelectronics" pp. 1-106 in Advances in Electronics and Electron Physics, Vol. 83, P. W. Hawkes, Ed., Academic Press: San Diego, 1992. *b.* C. A. Spindt, C. E. Holland, A. Rosengreen, and I. Brodie, "Field-Emitter Arrays for Vacuum Microelectronics",

IEEE Trans. Electron Dev. 38(10), 2355-2363 (1991). *c.* C. A. Spindt, C. E. Holland, I. Brodie, J. B. Mooney, and E. R. Westerberg, "Field-Emitter Arrays Applied to Vacuum Fluorescent Display", *IEEE Trans. Electron Dev.* 36(1), 225-228 (1989).

2. S. Yang, F. Zhang, C. Stoffers, S. M. Jacobsen, C. J. Summers, P. N. Yocom, S. McClelland, "Characterization of Potential Low-Voltage Phosphors for Field Emission Devices", *Proc. SPIE - Int. Soc. Opt. Eng.* 2408, 194-199 (1995).

3. S. Itoh, T. Kimizuka, and T. Tonegawa, "Degradation Mechanism for Low Voltage Cathodoluminescence of Sulfide Phosphors", *J. Electrochem. Soc.* 136(6), 1819-1823 (1989).

4. S. Itoh, T. Niiyama, and M. Yokoyama, "Influence of Gases on the Field Emission", *J. Vac. Sci. Technol.* B11, 647-650 (1992).

5. *a.* L. Ozawa and S. Hayakawa, "A Study on Cathodoluminescence Intensities in the Range Below 3 kv", *J. Lumin.* 28, 327-335 (1983).

6. S. Itoh, T. Tonegawa, T. L. Pykosz, K. Morimoto, and H. Kukimoto, "Influence of Grinding and Baking Processes on the Luminescent Properties of Zinc Cadmium Sulfide Phosphors for Vacuum Fluorescent Displays", *J. Electrochem. Soc.* 134 (12), 3178-3181 (1987).

7. Efficiency data: a. K. Narita, A. Kagami, and Y. Mimura, "Behavior of Phosphors under Low Voltage Cathode Ray Excitation", *J. Electrochem. Soc.* 127 (8), 1794-1798 (1980). b. A. O. Dmitrienko and S. L. Shmakov, "The Efficiency of Low-Voltage Cathodoluminescence of Modified Zinc Oxide Crystallophosphors", *Inorganic Materials* 30 (4), 534-535 (1994). Threshold voltage: R. E. Shrader and S. F. Kaisel, "Excitation of Zinc Oxide Phosphors by Low-Energy Electrons", *J. Opt. Soc. Am.* 44 (2), 135-137 (1954).

8. R. Raue, A. T. Vink, and T. Welker, "Phosphor Screens in Cathode-Ray Tubes for Projection Television", *Philips Tech. Rev.* 44 (11/12), 335-347 (1989).

9. $NaY(WO_4)_2$ as a laser host: H. Yizong, G. Wang, X. Huang, Z. Luo, "The Emission and Structure of a New Laser Crystal Nd^{3+}:$NaY(WO_4)_2$", *Cryst. Res. Technol.* 29(2), 267-271 (1994). $NaY(WO_4)_2$ as an anti-Stokes phosphor host: *a.* F. Auzel and D. Pencile, "Comparison and Efficiency of Materials for Summation of Photons Assisted by Energy Transfer", *J. Lumin.* 8(1), 32-43 (1973). *b.* B. M. Tissue, L. Lu, L. Ma, W. Jia, M. L. Norton, W. M. Yen, "Laser-heated Pedestal Growth of Laser and IR-Upconverting Materials", *J. Cryst. Growth* 109, 323-328 (1991).

10. T. Takamori and L. D. David, "Controlled Nucleation for Hydrothermal Growth of Yttrium-Aluminum Garnet Powders", *Am. Ceram. Soc. Bull.* 65 (9), 1282-1286 (1986).

DISCLAIMER

11. E. D. Kolb and R. A. Laudise, "Phase Equilibria of $Y_3Al_5O_{12}$, Hydrothermal Growth of $Gd_3Ga_5O_{12}$, and Hydrothermal Epitaxy of Magnetic Garnets", *J. Cryst. Growth* 29, 29-39 (1975).

12. "Procédé de préparation d'oxydes métalliques complexes", French Patent 2,007,316 (1970, to Swiss Aluminium Ltd.)

13. T. Takahashi, "Columnar crystalline zinc silicate phosphor prepared by hydrothermal reaction", Japanese Patent 63,196,683 (1988).

14. M. N. Viswanathiah, J. A. K. Tareen, and T. R. Narayanan Kutty, "Hydrothermal Phase Equilibria Studies in Ln_2O_3-H_2O Systems and Synthesis of Cubic Lanthanide Oxides", *Mater. Res. Bull.* 15(7), 855-859 (1980).

15. *a.* R. C. Ropp and B. Carroll, "Yttrium Phosphate-Yttrium Vanadate Solid Solutions and Vegard's Law", *Inorg. Chem.* 14(9), 2199-2202 (1975). *b.* O. Yamaguchi, Y. Mukaida, H. Shigeta, H. Takemura, and M. Yamashita, "Preparation of Alkoxy-Derived Yttrium Vanadate", *J. Electrochem. Soc.* 136(5), 1557-1560 (1989). *c.* H. J. Kaunders, "Europium-doped Yttrium Vanadate(V) Phosphor Preparation by Precipitation", U. S. Patent 3,479,296 (1969, to General Electric). *d.* M. L. F. Phillips, "Low-Voltage Cathodoluminescence of Europium-Activated Yttrium Orthovanadate", *Proc. SPIE - Int. Soc. Opt. Eng.* 2408, 200-206 (1995).

16. R. C. Ropp, The Chemistry of Artificial Lighting Devices, pp. 502-504, Elsevier: Amsterdam, 1993.

17. L. Ozawa, Cathodoluminescence, pp. 20-21, VCH Publishers: New York, 1990.

18. *a.* L. Ozawa and H. N. Hersh, "Random-Walk Model of Energy Transfer in Cathodoluminescence", *Phys. Rev. Lett.* 36(12), 683-686 (1976). *b.* L. Ozawa, "An Experimental Proof of Radiative Recombination Mechanisms of Electron-Hole Pairs at Activator Ions", *J. Electrochem. Soc.* 128(1), 140-145 (1981).

19. M. L. F. Phillips and B. G. Potter, unpublished results.